Available online at www.sciencedirect.com
SCIENCE DIRECT®
International Journal of Heat and Fluid Flow 24 (2003) 454–462
International Journal of HEAT AND FLUID FLOW
www.elsevier.com/locate/ijhff

Extensions of the Spalart–Allmaras turbulence model to account for wall roughness

B. Aupoix [a,*], P.R. Spalart [b]

[a] ONERA/DMAE Centre d'Études et de Recherches de Toulouse, B.P. 4025, 2, Avenue Édouard Belin, 31055 Toulouse Cedex 4, France
[b] Boeing Commercial Airplanes, P.O. Box 3707, Seattle, WA 98124, USA

Received 23 November 2002; accepted 15 March 2003

Abstract

This paper describes extensions of the Spalart–Allmaras model to surface roughness, developed independently by Boeing and ONERA. They are rather simple and numerically benign, yield similar predictions, and are in fair agreement with experiments. They do not provide a description of the flow near the roughness elements, but rely instead on the "equivalent sand grain" approach. In that sense, they are not self-contained. The uncertain accuracy of the separate correlations, such as Dirling's, needed to determine the sand grain size presents a challenge, as always. The roughness height must be much smaller than the boundary layer thickness, but the full range of roughness Reynolds number is covered. Some test cases reveal an incompatibility between the predicted effect of roughness on heat transfer and on skin friction. i.e. if the sand grain size is adjusted for skin friction, the heat transfer is too high.

Keywords: Boundary layer; Equivalent sand grain; Heat transfer; Pressure gradient; Skin friction; Turbulence modelling; Wall roughness

1. Extension of the Spalart–Allmaras model

1.1. Basic Spalart–Allmaras model

The Spalart–Allmaras (S–A) turbulence model solves only one transport equation for the quantity $\tilde{\nu}$, which is equivalent to the eddy viscosity ν_t far from walls. The transport equation has been constructed empirically to reproduce flows of increasing complexity. The transport equation, neglecting transition terms, reads (Spalart and Allmaras, 1994)

$$\frac{D\tilde{\nu}}{Dt} = c_{b1}\widetilde{S}\tilde{\nu} - c_{w1}f_w\left(\frac{\tilde{\nu}}{d}\right)^2 + \frac{1}{\sigma}[\mathrm{div}([\tilde{\nu}+\nu]\underline{\mathrm{grad}}\,\tilde{\nu}) + c_{b2}\underline{\mathrm{grad}}\,\tilde{\nu}\cdot\underline{\mathrm{grad}}\,\tilde{\nu}] \quad (1)$$

where d is the distance to the nearest wall. The model has been tuned so that, close to solid surfaces but outside the viscous region, it fits the logarithmic region, i.e.

$$\tilde{\nu} = u_\tau\kappa d, \quad \widetilde{S} = \frac{u_\tau}{\kappa d} \quad (2)$$

where u_τ is the friction velocity based upon the wall friction τ_w ($u_\tau = \sqrt{\tau_w/\rho}$) and κ the von Kármán constant. The turbulent viscosity ν_t is linked to the transported variable $\tilde{\nu}$ by

$$\nu_t = f_{v1}\tilde{\nu}, \quad f_{v1} = \frac{\chi^3}{\chi^3 + c_{v1}^3}, \quad \chi = \frac{\tilde{\nu}}{\nu} \quad (3)$$

and $\widetilde{S}$ is linked to the vorticity S (which reduces to $|\partial u/\partial y|$ in thin shear flows), by

$$\widetilde{S} = S + \frac{\tilde{\nu}}{\kappa^2 d^2}f_{v2}, \quad f_{v2} = 1 - \frac{\chi}{1+\chi f_{v1}} \quad (4)$$

Finally, f_w is a function of the ratio $r \equiv \tilde{\nu}/(\widetilde{S}\kappa^2 d^2)$, and both equal unity in the log layer. Eq. (1) is in balance provided $c_{w1} = c_{b1}/\kappa^2 + (1+c_{b2})/\sigma$.

1.2. Modelling roughness effects

It is assumed that the roughness-element size in any direction is small compared with the boundary layer thickness so that, above the roughnesses, the flow is averaged over numerous roughness elements the exact location of which is not accounted for. Two such "macroscopic" strategies can then be used to account

* Corresponding author. Tel.: +33-5-6225-2804; fax: +33-5-6225-2583.
E-mail address: bertrand.aupoix@onecert.fr (B. Aupoix).

0142-727X/03/$ - see front matter © 2003 Elsevier Science Inc. All rights reserved.
doi:10.1016/S0142-727X(03)00043-2

Nomenclature

C_f	skin friction coefficient $C_f = \tau_w/((1/2)\rho U_e^2)$
d	distance to the nearest wall
d_0	offset in the wall distance to account for wall roughness
h	roughness height
h_s	equivalent sand grain roughness height
S	vorticity
$\widetilde{S}$	transformed vorticity
u	longitudinal velocity component
u_τ	friction velocity
y	distance along the wall normal
Greeks	
δ	boundary layer thickness
κ	von Kármán constant
ν	viscosity
$\tilde{\nu}$	transported quantity in the S–A model
ν_t	turbulent eddy viscosity
ρ	density
τ_w	wall friction
Symbols	
$^+$	variable in wall scaling
e	value at the boundary layer edge
rough	value for a rough surface
smooth	value for a smooth surface
w	wall value

for wall roughness in Navier–Stokes computations, without solving the flow equations around each roughness element (see e.g. Patel (1998)). In both strategies, the boundary of the calculation domain is smooth, and the velocity boundary condition is zero.

- The "discrete element approach" accounts for the roughness by extra terms in the flow equations which represent the flow blockage due to the roughnesses and the drag and heat flux on roughness elements (see, e.g. Coleman et al. (1983) or Aupoix (1994) for the derivation of the equations). This approach requires drastic changes in the flow equations and has rarely been used in practical applications.
- The "equivalent sand grain approach' links the real roughness to an idealized roughness, with reference to Nikuradse's experiments (1933), the height of the equivalent sand grain being deduced from the real roughness shape with the help of empirical correlations, usually the correlation proposed by Dirling (1973) and Grabow and White (1975). The roughness effect is mimicked by increasing the turbulent eddy viscosity in the wall region to obtain higher skin friction and wall heat flux levels. Here again, two kinds of model can be considered:
  - Models in which the eddy viscosity is null at the boundary. They can be interpreted as models in which the virtual "wall" corresponds to the bottom of the roughnesses. The roughness correction then mainly acts through a reduction of the turbulence damping in the wall region.
  - Models in which the eddy viscosity is finite at the boundary. They can be interpreted as models in which the virtual wall is located part-way up the roughnesses. Unpublished studies at ONERA have shown that this approach better accounts for small roughnesses.

The increase in skin friction due to wall roughness can be directly related to changes in the velocity profiles, as will be shown in Fig. 9 where the profile is plotted in wall variables i.e. the normalized velocity $u^+ = u/u_\tau$ versus the normalized wall distance $y^+ = yu_\tau/\nu$. For high enough Reynolds numbers and at heights much larger than the roughness height, the logarithmic region and the outer layer or "wake" are simply shifted compared to the smooth-wall case. Accordingly, the roughness modifications of the models vanish in those regions. It must be remembered that the edge value of the normalized velocity is

$$u_e^+ = \frac{u_e}{u_\tau} = \sqrt{\frac{2}{C_f}} \tag{5}$$

so that, to first order, as the wake shape is unaffected by roughness, the increase in the skin friction coefficient C_f is directly related to the downward shift Δu^+ of the profile. Conversely, the effect of riblets would be an upward shift and a reduction of C_f (see e.g. Baron and Quadrio (1993)).

Nikuradse (1933) provided relations between this shift Δu^+ and the normalized roughness height $h_s^+ = h_s u_\tau/\nu$ for the specific sand grain roughnesses of various heights h_s he investigated. Once the shape of the sand or other roughness element is set, the classical analysis of the turbulent boundary layer leads directly to such a $\Delta u^+(h_s^+)$ relationship.

As a result, good predictions can be achieved only if the shift Δu^+ of the velocity profile is reproduced for any normalized sand grain roughness height h_s^+ *and* the equivalent sand grain roughness h_s is correctly estimated from the true shape of the considered rough surface. This estimate is far from trivial, and note that for most types of "real-life" roughness, the sand grain size h_s is several times larger than the depth of the grooves

or other irregularities that have the same effect on the velocity profile. Ignoring this would lead to a severe under-estimate of roughness effect in some cases.

1.3. Boeing extension

This extension (Spalart, 2000) was designed in the same spirit as the original model and to preserve its behaviour in the wall region (Eq. (2)) but non-zero values of $\tilde{\nu}$ and ν_t are now expected at the wall to mimic roughness effects. For that, the wall condition $\tilde{\nu} = 0$ is replaced by

$$\frac{\partial \tilde{\nu}}{\partial n} = \frac{\tilde{\nu}}{d} \tag{6}$$

where n is along the wall normal and the distance d has to be increased. The simplest way is to impose an offset $d = d_{\min} + d_0$ where $d_{\min}$ is the distance to the wall and $d_0(h_s)$ a length that will be adjusted. It will be a simple linear relationship, and the viscous functions of the model will be calibrated in the finite-Reynolds-number régime.

For very rough surfaces, in the fully rough regime ($h_s^+ > 70$), Nikuradse has shown that the velocity profiles, in the logarithmic region, obey

$$u^+ = \frac{1}{\kappa} \ln \frac{y}{h_s} + 8.5 \tag{7}$$

The molecular viscosity ν does not appear.

As the roughness effect is strong, the eddy viscosity should be large compared to the gas viscosity even at the wall, and $\nu_t = \tilde{\nu}$. Therefore, the momentum equation reduces to

$$u_\tau^2 = \nu_t \frac{\partial u}{\partial y} = u_\tau \kappa d \frac{\partial u}{\partial y} \tag{8}$$

the solution of which reads

$$u^+ = \frac{1}{\kappa} [\ln(y + d_0) - \ln(d_0)] \tag{9}$$

Identification of these two velocity profile expressions yields

$$d_0 = \exp(-8.5\kappa) h_s \approx 0.03 h_s \tag{10}$$

To achieve good predictions for smaller roughnesses, the f_{v1} function in Eq. (3) is altered by modifying χ as

$$\chi = \frac{\tilde{\nu}}{\nu} + c_{R1} \frac{h_s}{d}, \quad c_{R1} = 0.5 \tag{11}$$

This definition and value of c_{R1} give a dependence of Δu^+ on h_s^+ which is close to that given by Schlichting (1979) after Nikuradse.

The balance of the transport equation imposes that all terms have the same behaviour with respect to d as for smooth surfaces, so that the definition of $\widetilde{S}$ is unchanged

$$\widetilde{S} = S + \frac{\tilde{\nu}}{\kappa^2 d^2} f_{v2}, \quad f_{v2} = 1 - \frac{\tilde{\nu}}{\nu + \tilde{\nu} f_{v1}} \tag{12}$$

Regrettably, there is a misprint in the expression of f_{v2} in Spalart (2000).

1.4. ONERA extension

As previous unpublished ONERA studies have favored models using a non-zero value of the wall turbulent viscosity, especially for intermediate roughness heights, it was decided to impose such a value for $\tilde{\nu}$ to simulate wall roughness effects.

The required wall value was determined by solving the one-dimensional problem in the wall region. Neglecting advection, Eq. (1) reads, in wall variables, i.e. making terms dimensionless with the viscosity ν and the friction velocity u_τ

$$0 = c_{b1} \tilde{S}^+ \tilde{\nu}^+ - c_{w1} f_w \left(\frac{\tilde{\nu}^+}{d^+} \right)^2 + \frac{1}{\sigma} \left[\frac{\partial}{\partial y^+} \left(\tilde{\nu}^+ \frac{\partial \tilde{\nu}^+}{\partial y^+} \right) + c_{b2} \left(\frac{\partial \tilde{\nu}^+}{\partial y^+} \right)^2 \right] \tag{13}$$

while the momentum equation reduces to

$$\frac{\partial u^+}{\partial y^+} - \langle u'v' \rangle^+ = (1 + \nu_t^+) \frac{\partial u^+}{\partial y^+} = 1 \tag{14}$$

At the wall, the value of $\tilde{\nu}^+$ is imposed. The other boundary condition is imposed far in the logarithmic region where Eq. (14) reduces to $\tilde{\nu}^+ = \nu_t^+ = \kappa y^+ - 1$. Eq. (13) is solved using a pseudo-unsteady approach. The velocity gradient which appears through $\widetilde{S}$ is deduced from Eq. (14). Once a solution is obtained for $\tilde{\nu}$ and $\widetilde{S}$, the velocity profile can be deduced by simple integration, and the shift Δu^+ is determined.

It turned out that even imposing very large wall values for $\tilde{\nu}^+$ yielded small values of the velocity shift as the sink term $-c_{w1} f_w (\tilde{\nu}/d)^2$ in the transport equation became large and suppressed the effect of the imposed wall condition. An offset in the wall distance d has to be introduced. To be consistent with the behaviour over smooth walls, the distance d is expressed as

$$d^+ = d_{\min}^+ + \frac{\tilde{\nu}_w^+}{\kappa} \tag{15}$$

where $\tilde{\nu}_w$ is the imposed wall value for $\tilde{\nu}$. This new boundary condition preserves the solution

$$\tilde{\nu}^+ = \kappa d^+ \tag{16}$$

which is still the solution of Eqs. (13) and (14). Therefore, the solutions over smooth and rough walls are linked by

$$[\tilde{\nu}^+(y^+)]_{\text{rough}} = \left[\tilde{\nu}^+ \left(y^+ + \frac{\tilde{\nu}_w^+}{\kappa} \right) \right]_{\text{smooth}} \tag{17}$$

and the same relation holds for the velocity profile so that the velocity shift reads

$$\Delta u^+ = \left[u^+\left(\frac{\tilde{\nu}_w^+}{\kappa}\right)\right]_{\text{smooth}} \tag{18}$$

This allows to get analytical relationships between the wall eddy viscosity and the equivalent sand grain roughness for mildly rough surfaces $\left(\tilde{\nu}_w^+/\kappa < 3\right)$ and for very rough surfaces $\left(\tilde{\nu}_w^+/\kappa > 50\right)$. These relations are used to build the final model form:

$$\begin{aligned}\tilde{\nu}_w^+ = {} & (0.377 \ln h_s^+ - 0.447)\exp\left(-\frac{h_s^+}{70}\right) \\ & + 1.25710^{-2} h_s^+ \left[1 - \exp\left(-\frac{h_s^+}{70}\right)\right] \\ & + \max\left(0; \log\frac{h_s^+}{10}\right) \min\left(1; 1.36\exp\left(-\frac{h_s^+}{250}\right); \right. \\ & \left. 25\exp\left(-\frac{h_s^+}{100}\right)\right)\end{aligned} \tag{19}$$

1.5. Comparison of the two extensions

The Boeing model only refers to the sand grain roughness height, whereas the ONERA model also needs the friction velocity. This leads to different behaviours close to two-dimensional separation where the friction velocity tends to zero. The Boeing model then predicts stronger effects of the wall roughness. It must be pointed out that the ONERA model leads to no numerical problem at separation: u_τ is null, and so is h_s^+ and hence $\tilde{\nu}_w$ and d_0.

Both extensions change the wall boundary condition, either imposing the wall value or providing a mixed condition. In both cases, the wall distance d is modified so that the model is non-local: the information about the offset d_0 has to be known, i.e. each field point has to be related to a point on the surface. This represents a slight but unfortunate deviation from the "charter" of the S–A model. The Boeing change of d is simpler in that it only depends upon the roughness height and remains the same during computational iterations. Finally, the Boeing model requires changing the expression of χ in the damping function f_{v1}.

2. Validation

Both extensions have been implemented in the ONERA two-dimensional boundary layer code CLIC2 and compared to other roughness models such as mixing length model (van Driest, 1956; Rotta, 1962; Krogstad, 1991), k–ε models (Blanchard, 1977) or k–ω model (Wilcox, 1988) for various experiments. The results of other models, which are either irrelevant or very close to the present ones, are not given here for the sake of clarity of the figures. Only a selection of pertinent test-cases is reported. In all figures, the solid line corresponds to the prediction of the S–A model over a smooth-wall, to highlight roughness effects.

Unless otherwise specified, the equivalent sand grain roughness is deduced from Dirling's correlation which links the sand grain roughness h_s to the mean roughness height h as

$$\begin{aligned} h &= \alpha h_s \quad \alpha = \begin{cases} 60.95\Lambda^{-3.78} & \text{if } \Lambda < 4.915 \\ 0.0072\Lambda^{1.9} & \text{if } \Lambda > 4.915 \end{cases} \\ \Lambda &= \frac{L}{h}\left(\frac{A_s}{A_p}\right)^{4/3} \end{aligned} \tag{20}$$

where

- h is the mean roughness height,
- L is the mean distance between roughness elements, i.e. if there are N roughness elements on an area S, $L = \sqrt{S/N}$,
- A_p is the surface of the roughness projected on a plane normal to the flow direction,
- A_s is the wetted surface of the roughness directly exposed to the upstream flow.

Initial profiles are generated automatically by the code from the prescribed value of the momentum thickness, assuming local self-similarity and using a mixing length model which accounts for wall roughness. The quantity $\tilde{\nu}$ is then deduced from the eddy viscosity.

2.1. Blanchard's experiments

Blanchard (1977) conducted experiments over various surfaces, including sand grain paper of various heights and wire meshes. We present predictions for a sand grain paper the average height of which is 0.425 mm. Blanchard estimated that the equivalent sand grain roughness height was twice the height of his roughness. This is not fully consistent with the equivalent sand grain roughness which can be deduced from Dirling's correlation and the simplified surface representation Blanchard proposed using cones, but he pointed to the large scatter in the correlation.

The first case corresponds to a zero pressure gradient flow, with an external velocity of 45 m s^{-1}. This gives a normalized equivalent sand grain roughness height h_s^+ about 150, i.e. a fully rough regime. Both models predict a skin friction evolution in fair agreement with experiments as shown in Fig. 1. The Boeing extension gives slightly higher predictions. For a rougher surface, velocity profiles predicted by both extensions are indistinguishable and in fair agreement with experiments. Recall that the models were not calibrated on this flow.

Fig. 2 shows predictions for a positive pressure gradient flow. As the pressure gradient is moderate, the friction velocity does not decrease much, and normalized

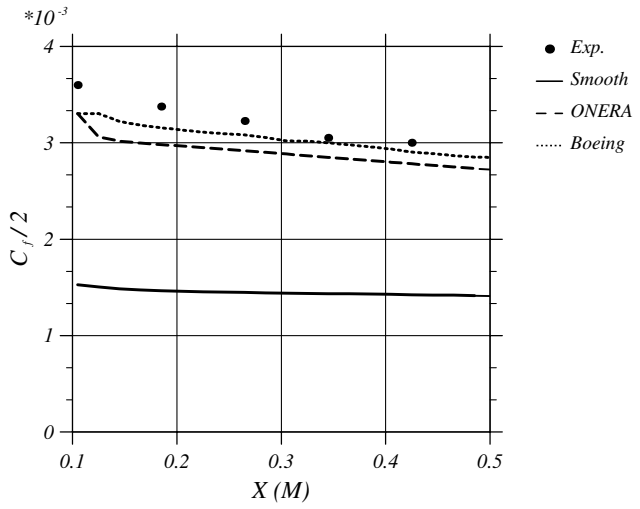

Fig. 1. Skin friction predictions—Blanchard 0.425 mm case—zero pressure gradient flow.

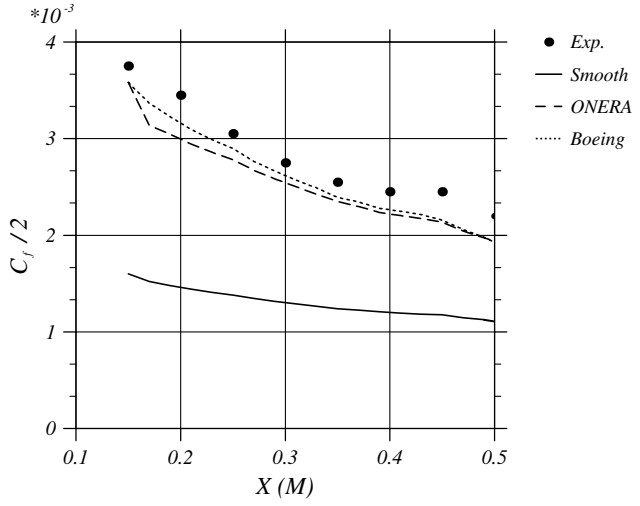

Fig. 2. Skin friction predictions—Blanchard 0.425 mm case—positive pressure gradient flow.

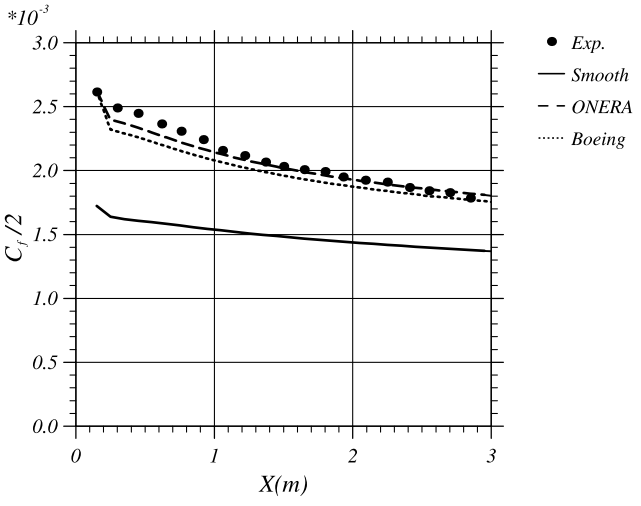

Fig. 3. Skin friction predictions—Acharya et al. SRS1 surface—$U = 19\ \mathrm{m\,s^{-1}}$—zero pressure gradient flow.

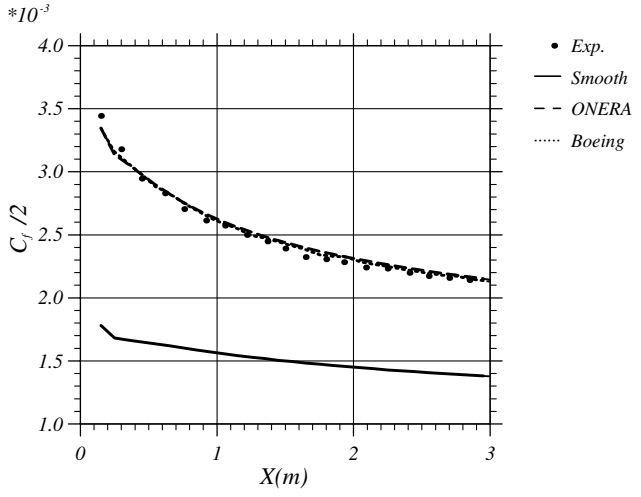

Fig. 4. Skin friction predictions—Acharya et al. SRS2 surface—$U = 19\ \mathrm{m\,s^{-1}}$—zero pressure gradient flow.

equivalent sand grain roughness height h_s^+ remains about 150. The agreement with experiment remains good, and the discrepancy between the models is smaller.

2.2. Acharya et al. experiments

Acharya et al. (1986) conducted experiments on surfaces specifically machined to reproduce aged turbine blade surfaces. Two surfaces, named SRS1 and SRS2 for "simulated rough surface" have been considered, for a constant external velocity of $19\ \mathrm{m\,s^{-1}}$. Equivalent sand grain roughness heights have been evaluated from Dirling's correlation and surface statistics given in Tarada's thesis (1987).

Surface SRS1 gives a normalized equivalent sand grain roughness height h_s^+ about 25, i.e. a transitionally rough regime. Fig. 3 shows that both models predict the skin friction fairly well, the ONERA model giving higher values and therefore better agreement.

Surface SRS2 gives a normalized equivalent sand grain roughness height h_s^+ about 70, i.e. the lower limit of the fully rough regime. Fig. 4 shows that both models are in excellent agreement with experiments.

2.3. MSU experiments

Many experiments over rough surfaces have been performed at Mississippi State University (MSU). Hosni et al. (1993, 1991) investigated boundary layers over spheres, hemispheres and cones arranged in staggered rows in a low-speed wind tunnel designed to perform heat transfer measurements. Skin friction was deduced

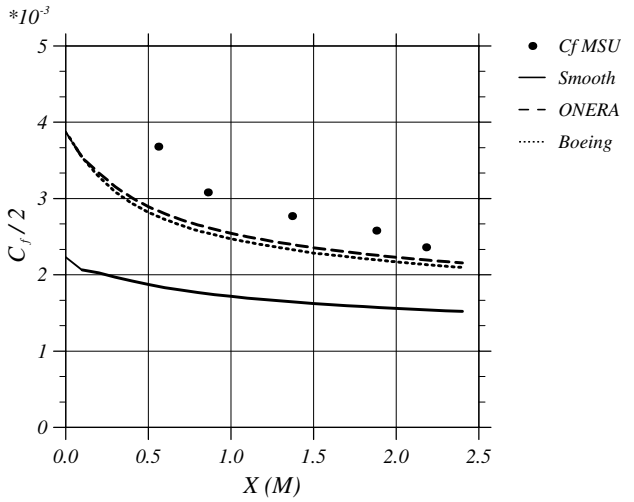

Fig. 5. Skin friction predictions—MSU experiment—hemispheres with spacing/height ratio of two—$U = 12\ \mathrm{m\,s^{-1}}$.

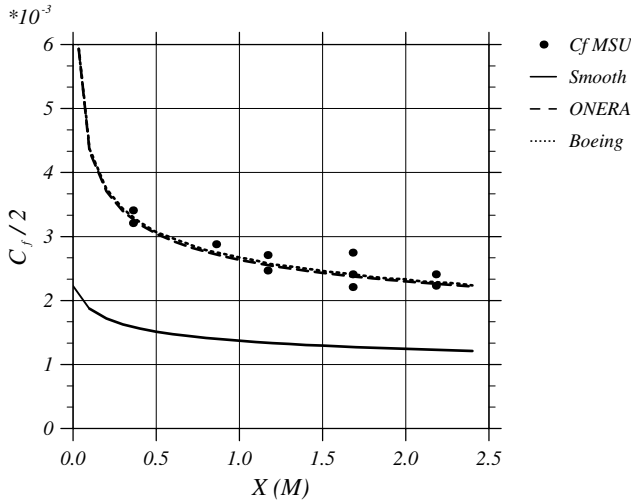

Fig. 7. Skin friction predictions—MSU experiment—hemispheres with spacing/height ratio of two—$U = 58\ \mathrm{m\,s^{-1}}$.

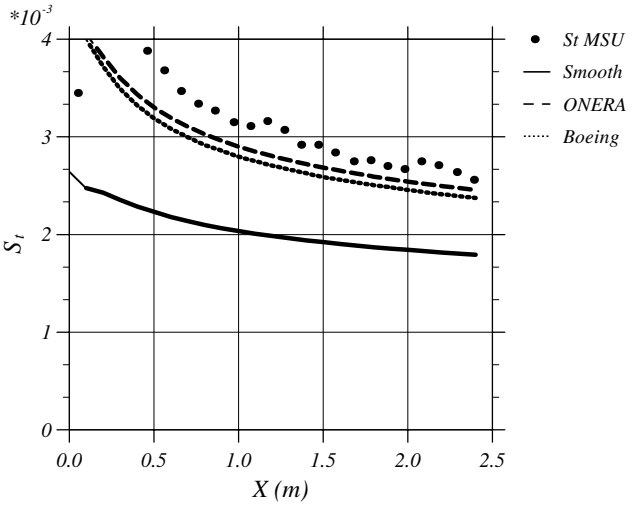

Fig. 6. Stanton number predictions—MSU experiment—hemispheres with spacing/height ratio of two—$U = 12\ \mathrm{m\,s^{-1}}$.

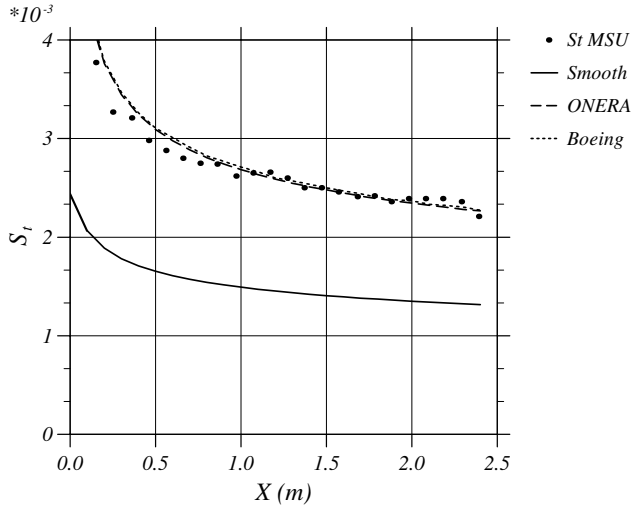

Fig. 8. Stanton number predictions—MSU experiment—hemispheres with spacing/height ratio of two—$U = 58\ \mathrm{m\,s^{-1}}$.

from the Reynolds stress $\langle -u'v' \rangle$ above the roughnesses, corrected via a momentum balance around the roughnesses. The data were in fair agreement with the skin friction estimate from the von Kármán equation. Heat fluxes were deduced from an energy balance for each heated wall plate, accounting for losses by conduction and radiation.

Only results for hemispheres, 1.27 mm in diameter, will be presented here. The case of a spacing-over-height ratio of ten, i.e. for a weakly rough surface, is not presented here. All test cases are for zero pressure gradient flows. The equivalent sand grain height h_s is determined from Dirling's correlation.

The first surface is covered with hemispheres with a spacing of twice their height. For an external velocity of $12\ \mathrm{m\,s^{-1}}$, the normalized equivalent sand grain roughness height h_s^+ is about 45, i.e. a transitionally rough regime. Both extensions under-predict both the skin friction and the Stanton number, as shown in Figs. 5 and 6. Other roughness models yield similar predictions. Here again, the ONERA extension gives slightly higher and better levels than the Boeing one.

When the velocity is increased to $58\ \mathrm{m\,s^{-1}}$, the normalized equivalent sand grain roughness height h_s^+ is about 220, i.e. a fully rough regime. Then, the agreement between predictions and measurements is excellent as shown in Figs. 7 and 8.

The velocity profiles in wall variables are plotted in Fig. 9. The shift Δu^+ of the logarithmic region and of the wake is about ten wall units. Both models give similar profiles, except very close to the wall where the notion of mean velocity profile makes limited sense.

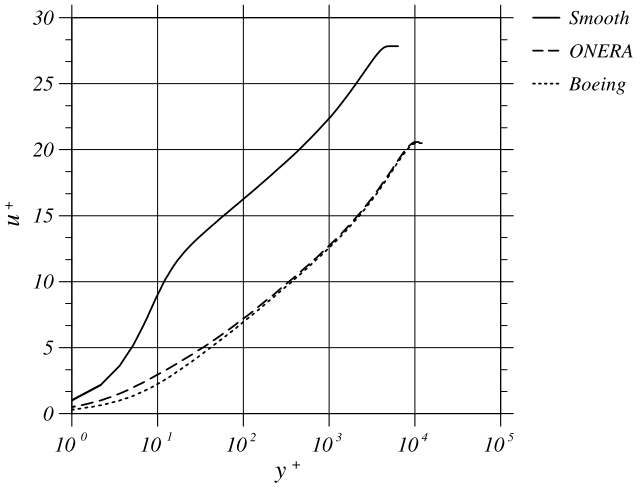

Fig. 9. Semi-log plot of the velocity profiles predictions—MSU experiment—hemispheres with spacing/height ratio of two—$U = 58\ \mathrm{m\,s^{-1}}$.

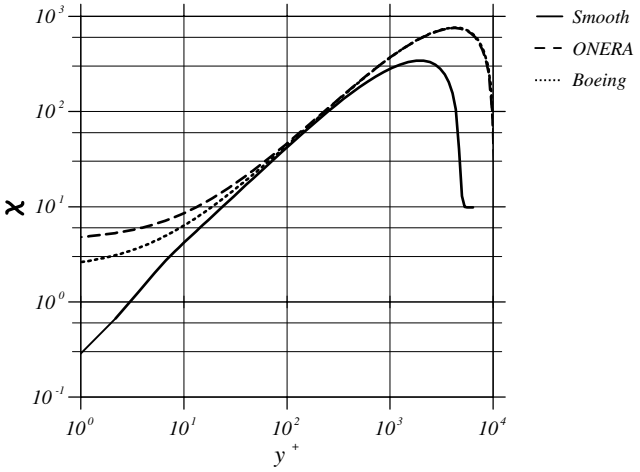

Fig. 10. Logarithmic representation of $\chi = \tilde{\nu}/\nu$ predictions—MSU experiment—hemispheres with spacing/height ratio of two—$U = 58\ \mathrm{m\,s^{-1}}$.

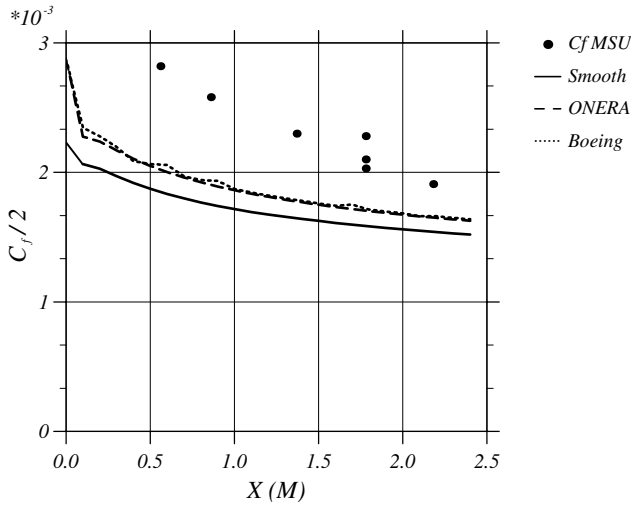

Fig. 11. Skin friction predictions—MSU experiment—hemispheres with spacing/height ratio of four—$U = 12\ \mathrm{m\,s^{-1}}$.

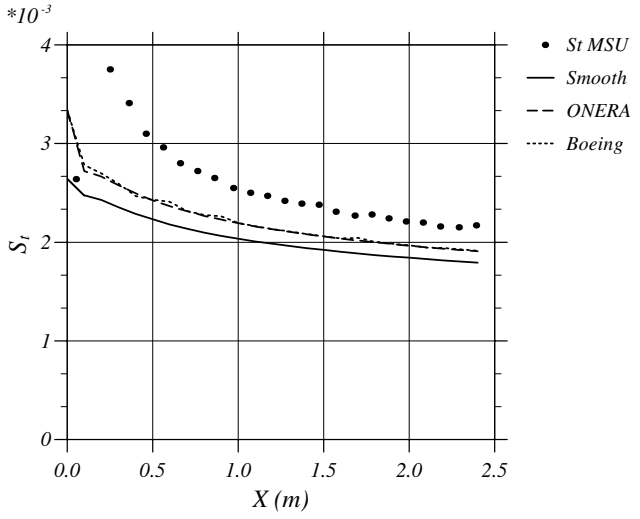

Fig. 12. Stanton number predictions—MSU experiment—hemispheres with spacing/height ratio of four—$U = 12\ \mathrm{m\,s^{-1}}$.

Fig. 10 illustrates the increase of the quantity $\tilde{\nu}$ in the wall region. The two models take somewhat different values at the wall. In the logarithmic and wake region, they give similar eddy viscosity levels, reaching more than twice the level on a smooth surface. The eddy viscosity is the product of a turbulence velocity scale, which is proportional to the friction velocity u_τ, and a turbulence length scale which is linked, in the outer region, to the boundary layer thickness. Therefore the eddy viscosity increase is due to both increases of the friction level and of the boundary layer thickness.

The second surface is covered with hemispheres with a spacing of four times their height. For an external velocity of 12 $\mathrm{m\,s^{-1}}$, the normalized equivalent sand grain roughness height h_s^+ is about 10, i.e. a transitionally rough regime. Both extensions give identical results but under-predict both the skin friction and the Stanton number, as shown in Figs. 11 and 12. Other roughness models yield similar predictions.

When the external velocity is increased to 58 $\mathrm{m\,s^{-1}}$, the normalized equivalent sand grain roughness height h_s^+ is about 50, i.e. a transitionally rough regime similar to the first MSU case, but for a higher range of values of the Reynolds number R_θ based upon the boundary layer momentum thickness. As for the first MSU case, the skin friction is under-estimated while the Stanton number is fairly well reproduced (Figs. 13 and 14).

Both extensions give similar predictions, whatever the roughness regime. Which extension gives a slightly higher skin friction depends upon the normalized

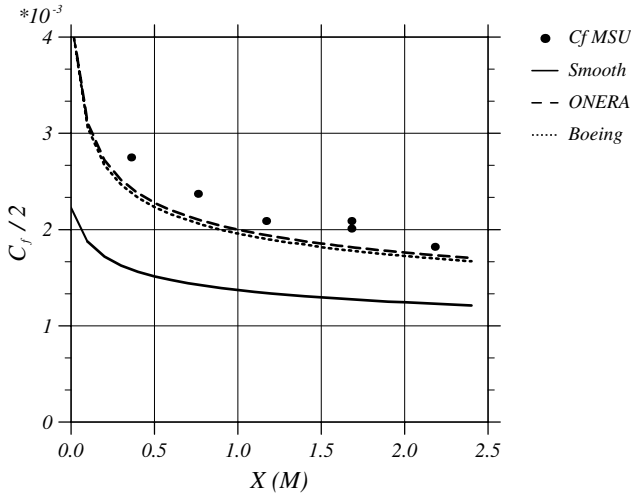

Fig. 13. Skin friction predictions—MSU experiment—hemispheres with spacing/height ratio of four—$U = 58\ \mathrm{m\,s^{-1}}$.

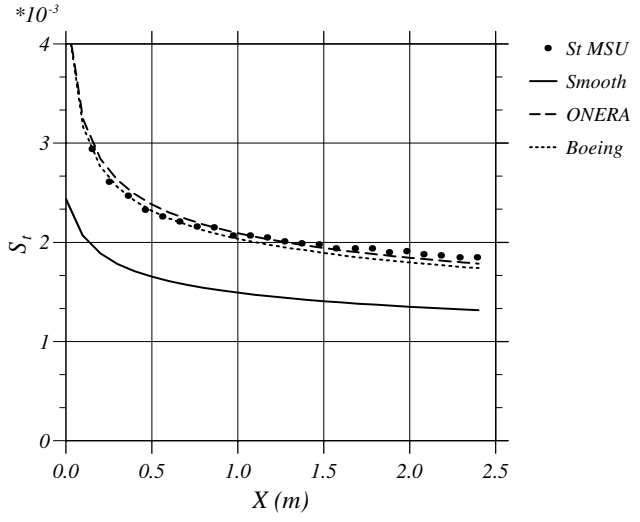

Fig. 14. Stanton number predictions—MSU experiment—hemispheres with spacing/height ratio of four—$U = 58\ \mathrm{m\,s^{-1}}$.

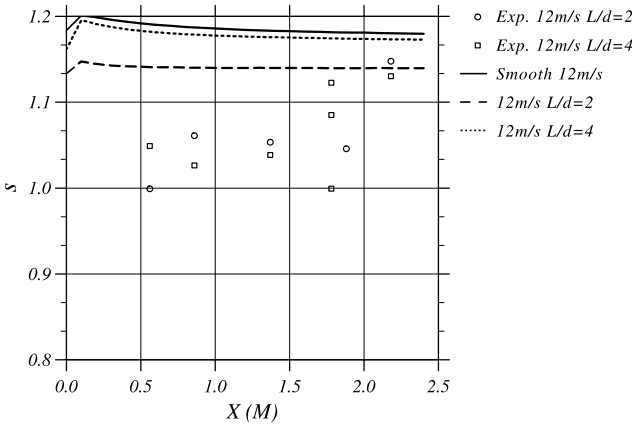

Fig. 15. Analogy factor predictions—MSU experiment—$U = 12\ \mathrm{m\,s^{-1}}$.

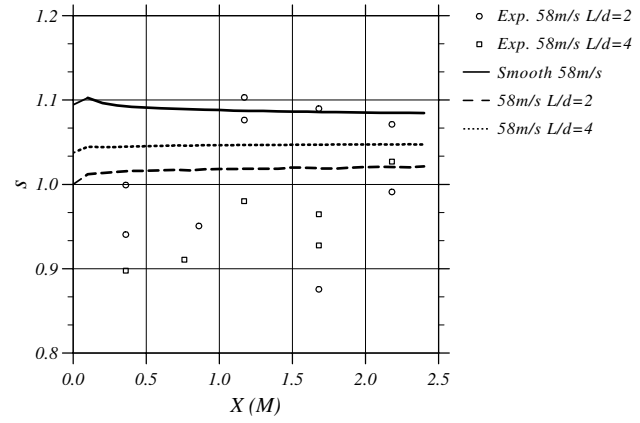

Fig. 16. Analogy factor predictions—MSU experiment—$U = 58\ \mathrm{m\,s^{-1}}$.

equivalent sand grain roughness height h_s^+. The predictions are comparable to those of the best tested roughness models, again showing that having a single equation is not a serious obstacle to useful modelling. As regards the MSU experiments, for high values of h_s^+, predictions are in good agreement with experiments while roughness effects are under-estimated for the same surfaces in the transitionally rough regime. However, good predictions are achieved in the transitionally rough regime for the Acharya et al. experiments. Either the relation $\Delta u^+(h_s^+)$ proposed by Nikuradse and which has been used to calibrate models is failing and the good predictions in the transitionally rough regime are incidental, or a given roughness does not correspond always to the same equivalent sand grain roughness height, which means that the correlations are not accurate and complete enough.

A closer inspection of the predictions reveals that the heat transfer increase due to roughnesses is overestimated compared to the skin friction increase. A striking example is the last test-case for which the skin friction is under-estimated while the Stanton number is fairly well predicted. This is a well-known drawback of the equivalent sand grain approach as the thermal and dynamical problems are solved similarly, the same increase being applied to the turbulent viscosity and conductivity. Assuming a linear relation between the velocity and total enthalpy profiles, the analogy factor s reads:

$$s = \frac{St}{C_f/2} \propto \frac{(\lambda + \lambda_t)\frac{\partial h_i}{\partial y}}{(\nu + \nu_t)\frac{\partial u}{\partial y}} \propto \frac{(\lambda + \lambda_t)}{(\nu + \nu_t)} \propto \frac{1}{P_m} \tag{21}$$

where P_m is a mixed Prandtl number which increases from the gas Prandtl number (0.72) for smooth surfaces to the turbulent Prandtl number (0.9) for fully rough surfaces. Figs. 15 and 16 show that, although there is

some scatter in the data, the decrease of the analogy factor is under-predicted by the models, compared with experiments, when the surface becomes rougher. This is consistent with Dipprey and Sabersky's results (1963) and the idea that the skin friction increase is mainly due to pressure drag on the roughnesses while the heat-transfer increase is a viscous phenomenon and is more closely linked to the wetted surface increase. Therefore, the Reynolds analogy no longer holds for rough surfaces, while the modelling implemented here still uses it. Corrections based on functions of d/h_s may be devised in the future.

3. Conclusion

Two extensions of the S–A turbulence model have been derived. Both assume a non-zero-eddy viscosity at the wall and change the definition of the distance d, so that the model becomes non-local. The Boeing extension only uses the roughness height while the ONERA also refers to the friction velocity. The modifications are rather minor. The extensions could be used instead of the original S–A f_{t1} term to trip boundary layers; a rough band would be placed along the transition line. However there is no decisive advantage over the f_{t1} form and the f_{t2} term would still be needed.

Tests on a variety of two-dimensional experiments show that these extensions give similar predictions, in fair agreement with other roughness models and, generally, with experiments. No test is available close enough to separation to differentiate the models for low skin friction levels. However, comparisons raise doubts about the universality of the equivalent sand grain size, which appears to depend upon the flow regime for a given surface. In other words, for a given roughness shape, the optimal sand grain roughness height h_s is not simply proportional to the physical size of the roughness. While h was expected to depend on flow direction, for instance with grooves, a dependence on the friction velocity is a further disappointment and inconvenience. Moreover, the over-prediction of roughness effects on heat transfer compared with the effects on skin friction, using the equivalent sand grain approach and a uniform turbulent Prandtl number, is unfortunately repeatable.

Acknowledgements

The ONERA work was divided between the ARCAE research program funded by the French Ministry of Defence and the research project "Unsteady Transitional Flows in Axial Turbomachines" funded by the European Commission under contract number G4RD-CT-2001-00628. It is the first author's pleasure to acknowledge P. Baubias and G. Fontaine for their contributions to this work.

References

Acharya, M., Bornstein, J., Escudier, M.P., 1986. Turbulent boundary layers on rough surfaces. Experiments in Fluids 4 (1), 33–47.

Aupoix, B., 1994. Modelling of boundary layers over rough surfaces. In: Benzi, R. (Ed.), Advances in Turbulence V, Sienna. Fifth European Turbulence Conference. Kluwer, pp. 16–20.

Baron, A., Quadrio, M., 1993. Some preliminary results on the influence of riblets on the structure of a turbulent boundary layer. International Journal of Heat and Fluid Flow 14 (3), 223–230.

Blanchard, A., 1977. Analyse Expérimentale et Théorique de la Structure de la Turbulence d'une Couche Limite sur Paroi Rugueuse. Ph.D. thesis, Université de Poitiers U.E.R.-E.N.S.M.A.

Coleman, H.W., Hodge, B.K., Taylor, R.P., 1983. Generalized roughness effects on turbulent boundary layer heat transfer—a discrete element predictive approach for turbulent flow over rough surfaces. Air Force Armament Laboratory AFATL-TR-83-90, Mississippi State University.

Dipprey, D.F., Sabersky, R.H., 1963. Heat and momentum transfer in smooth and rough tubes at various Prandtl numbers. International Journal of Heat and Mass Transfer 6, 329–353.

Dirling Jr., R.B., 1973. A method for computing rough wall heat transfer rates on reentry nosetips. AIAA Paper 73-763, AIAA 8th Thermophysics Conference, Palm Springs, California.

Grabow, R.M., White, C.O., 1975. Surface roughness effects on nosetip ablation characteristics. AIAA Journal 13 (5), 605–609.

Hosni, M.H., Coleman, H.W., Taylor, R.P., 1991. Measurements and calculations of rough-wall heat transfer in the turbulent boundary layer. International Journal of Heat and Mass Transfer 34 (4/5), 1067–1082.

Hosni, M.H., Coleman, H.W., Gardner, J.W., Taylor, R.P., 1993. Roughness element shape effects on heat transfer and skin friction in rough-wall turbulent boundary layer. International Journal of Heat and Mass Transfer 36 (1), 147–153.

Krogstad, P.Å., 1991. Modification of the van Driest damping function to include the effects of surface roughness. AIAA Journal 296, 888–894.

Nikuradse, J., 1933. Strömungsgesetze in rauhen Rohren. Tech. Rept 361, VDI-Forschungsheft.

Patel, V.C., 1998. Perspective: flow at high Reynolds number and over rough surfaces—Achilles heel of CFD. Journal of Fluids Engineering 120, 434–444.

Rotta, J., 1962. Turbulent boundary layers in incompressible flows. Progress in Aeronautical Sciences 2, 73–82.

Schlichting, H., 1979. Boundary-Layer Theory, seventh ed. McGraw-Hill, New York.

Spalart, P., 2000. Trends in turbulence treatments. AIAA Paper 2000-2306, Fluids 2000, Denver.

Spalart, P.R., Allmaras, S.R., 1994. A one-equation turbulence model for aerodynamic flows. La Recherche Aérospatiale 1, 5–21.

Tarada, F.H.A., 1987. Heat Transfer to Rough Turbine Blading. Ph.D. thesis, University of Sussex.

van Driest, E.R., 1956. On turbulent flow near a wall. Journal of Aeronautical Sciences 23 (11), 1007–1011.

Wilcox, D.C., 1988. Reassessment of the scale-determining equation for advanced turbulence models. AIAA Journal 26 (11), 1299–1310.